



HAL
open science

A multi-scale model of plasticity and damage for rock-like materials with pores and inclusions

Y.J. Cao, Wanqing Shen, Jian-Fu Shao, W. Wang

► **To cite this version:**

Y.J. Cao, Wanqing Shen, Jian-Fu Shao, W. Wang. A multi-scale model of plasticity and damage for rock-like materials with pores and inclusions. *International Journal of Rock Mechanics and Mining Sciences*, 2021, 138, pp.104579. 10.1016/j.ijrmms.2020.104579 . hal-03245211

HAL Id: hal-03245211

<https://hal.science/hal-03245211>

Submitted on 2 Jan 2023

HAL is a multi-disciplinary open access archive for the deposit and dissemination of scientific research documents, whether they are published or not. The documents may come from teaching and research institutions in France or abroad, or from public or private research centers.

L'archive ouverte pluridisciplinaire **HAL**, est destinée au dépôt et à la diffusion de documents scientifiques de niveau recherche, publiés ou non, émanant des établissements d'enseignement et de recherche français ou étrangers, des laboratoires publics ou privés.



Distributed under a Creative Commons Attribution - NonCommercial 4.0 International License

A multi-scale model of plasticity and damage for rock-like materials with pores and inclusions

Y.J. Cao^{1,2}, W.Q. Shen^{1,2}, J.F. Shao^{1,2*}, W. Wang¹

¹*Key Laboratory of Ministry of Education for Geomechanics and Embankment Engineering, Hohai University, Nanjing 210098, China*

²*University of Lille, CNRS, LaMcube, UMR9013, 59000 Lille, France*

**Corresponding author: jian-fu.shao@polytech-lille.fr*

Abstract

A multi-scale model is developed for modeling of plastic deformation and induced damage in rock-like materials containing pores and mineral inclusions. An analytical macroscopic plastic yield criterion is first determined from three steps of homogenization. This criterion explicitly takes into account respective effects of two populations of pores and mineral inclusions at three different scales. The accuracy of criterion is evaluated by comparisons with numerical results issued from direct simulations on representative volume elements. Then, an induced damage evolution law is defined to describe the onset and growth of micro-cracks inside the solid matrix of materials. The induced damage affects both elastic and strength properties of the solid matrix and its evolution is coupled with the plastic deformation. The performance of the proposed model is first assessed through a series of numerical examples, clearly showing influences of pores and inclusions on macroscopic responses of heterogeneous materials. Finally, the proposed model is applied to describe mechanical behaviors of clayey rocks. Comparisons between numerical results and experimental data are presented.

Keywords: Plasticity, Damage, Porosity, Mineral inclusions, Multi-scale, Homogenization, Rock-like materials

1. Introduction

Rock-like materials are natural heterogeneous continua with different kinds of multi-scale heterogeneities. Their macroscopic mechanical and physical properties are inherently affected by the presence and evolution of those heterogeneities. Experimental studies and numerical simulations have revealed empirical correlations of several mineralogical and textural characteristics [1, 2, 3, 4, 5, 6], and porosity [7, 8, 9, 10, 11] with the physical and mechanical properties of rocks. As a representative example, hard clayey rocks are specifically studied in this work. This class of rocks are widely involved in different engineering fields such as civil

and mining engineering, oil industry and especially unconventional hydrocarbon production, as well as geological disposal of nuclear waste. For instance, the Callovo-Oxfordian (COx) claystone is selected as the geological barrier of underground disposal of radioactive waste in France. Based on mineralogical and micro-structural analyses performed on the COx claystone [12, 13] and other clayey rocks [14], heterogeneities are embedded at several scales. Basically, at the mesoscopic scale, mineral grains (carbonate, quartz, kerogen) are embedded in a nearly continuous clay matrix. At the microscopic scale, there is a distribution of large pores and fine mineral particles. Finally, at the nanoscopic scale, small pores are embedded inside a solid phase composed of clay particle. As a first approximation, two populations of pores should be considered ranging from $1nm$ to $100\mu m$ [15]. The objective here is to develop a multi-scale model for modeling plastic deformation and induced damage in clayey rocks by considering two populations of pores and mineral inclusions at three representative scales.

The relationships between mineral compositions, textural parameters and macroscopic unconfined compressive strength have firstly been established by simple regression analyses. On the other hand, in the framework of micro-mechanics, a series of research works have been devoted to establishing analytical macroscopic strength criteria by using homogenization theories of heterogeneous materials and by considering mineral inclusions and pores at different scales [16, 17, 18, 19, 20]. The effective strength can be explicitly determined as a function of porosity and inclusions volume fraction. On the other hand, in order to consider geometrical effects (size and shape) of inclusions and pores, analytical and numerical methods are combined. For instance, closed-form solutions are used at the microscopic scale [21, 22] while computational homogenization methods are employed at the mesoscopic scale such as Finite Element Method [23, 24, 25]) and Fast Fourier Transform technique [26, 27, 9, 10]. With these methods, it is also possible to account for interactions between different kinds of heterogeneities at the same scale. Further, extended incremental methods are developed for describing full mechanical responses of rock-like materials containing mineral inclusions and pores [28].

However, most previous studies have mainly focused on the estimation of macroscopic strength or plastic behavior. In rock-like materials, damage due to micro-cracking is another important process to consider. In [29], a state of the art was presented on the strategies available to relate the micro-scale of crystals, cracks and pores to the scale of a Representative Elementary Volume. A high number of phenomenological plastic damage models have also been proposed in the framework of thermodynamics and continuum damage mechanics [30, 31, 32, 33, 34, 35]. The damage evolution is generally driven by stored elastic and plastic energy. But the physical origin of damage at the microscopic scale is not clearly identified. At the same time, micro-mechanical damage models have also been developed with the help

of linear homogenization methods for elastic brittle materials [36, 37, 38, 39]. These models are able to consider unilateral effects related to crack closure, damage-friction coupling, induced anisotropy [40, 41, 42, 43]. Some studies are focused on the nonlocal damage or gradient damage model [44, 45, 46, 47, 48], which provide an objective description of strain localization behavior. However, the influences of multi-scale characters of the rock-like materials such as pores and inclusions still require much more effort to take into account, since these characters play important roles on the macroscopic mechanical behavior.

The objective of the present study is to develop a micro-mechanics based constitutive model for plastic deformation and damage evolution in rock-like materials containing two populations of pores and mineral inclusions at three different scales. An analytical plastic yield criterion is first established by using a three-step homogenization procedure based on a modified secant method [22, 28]. A specific plastic hardening law is also proposed by combining the evolutions of porosity and frictional coefficient of the solid matrix. Further, a time-dependent damage law is introduced to describe the degradation of both the elastic and plastic properties of solid matrix. The proposed model is assessed through a series of numerical examples and comparisons with experimental data obtained on typical claystone and shale with different mineral compositions.

2. Microstructure and elastic properties of materials

In this study, we consider materials characterized by three representative scales, such as claystone and cement-based materials. At the mesoscopic scale, mineral inclusions (quartz and calcite grains, aggregates etc. of several hundreds of micrometers) are embedded into a matrix continuum (clay matrix or cement paste for example). At the microscopic scale, large pores (inter-particle pores of a few hundreds of nanometers to micrometers) are distributed inside the matrix phase. At the nanometric scale, small pores (intra-particle pores of a few nanometers) are found. Therefore, the typical representative volume element (RVE) of those materials can be characterized by three scale as shown in Fig.1. It is needed to homogenize the porous medium at the first two scales and the inclusion-reinforced composite material at the last scale. A three-step upscaling method should be developed. For the sake of simplicity, it is here assumed that all the inclusions and pores are of spherical form. Geometrical effects of pores and inclusions will be investigated in an extended study. One denotes ω as the total volume of the RVE, ω_i the volume of inclusions at the level 2, ω_m the volume of matrix phase at the level 2, ω_1 the volume of large pores at the level 1, ω_0 the volume of small pores at the level 0, and ω_s the volume of solid grains at the level 0. Thus, the volume fraction of inclusions ρ , the porosity of large pores ϕ at the level 1, the porosity f of small pores at the

level 0 and the total porosity Γ at the macroscopic scale can be given as:

$$\begin{aligned}\rho &= \frac{\omega_i}{\omega}, \quad \phi = \frac{\omega_1}{\omega_m} = \frac{\omega_1}{\omega_s + \omega_1 + \omega_0}, \quad f = \frac{\omega_0}{\omega_s + \omega_0} \\ \Gamma &= \frac{\omega_0 + \omega_1}{\omega} = [f(1 - \phi) + \phi](1 - \rho)\end{aligned}\quad (1)$$

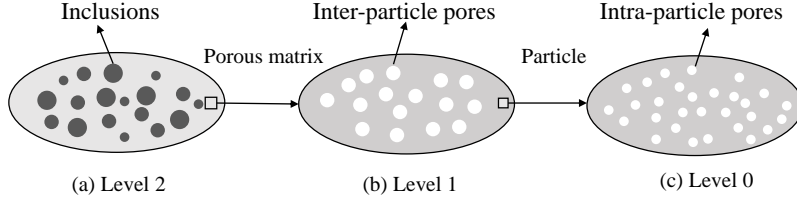


Figure 1: Representative volume element of studied rock-like materials

The effective macroscopic elastic properties of material are obtained by making three steps of homogenization with the standard [49] scheme. The effective elastic properties of the porous matrix ($\omega_s + \omega_0$) at the level 0, denoted as κ_{m0} and μ_{m0} , are given by the first step of homogenization:

$$\kappa_{m0} = \frac{4(1-f)\kappa_s\mu_s}{4\mu_s + 3f\kappa_s}; \quad \mu_{m0} = \frac{(1-f)\mu_s}{1 + 6f\frac{\kappa_s + 2\mu_s}{9\kappa_s + 8\mu_s}} \quad (2)$$

where κ_s and μ_s are the bulk and shear moduli of the solid phase. By making a second step of homogenization, the effective elastic properties of the porous matrix ($\omega_1 + \omega_s + \omega_0$) at the level 1 can be determined and denoted as κ^{pm} , μ^{pm} :

$$\kappa^{pm} = \frac{4(1-\phi)\kappa_{m0}\mu_{m0}}{4\mu_{m0} + 3\phi\kappa_{m0}}; \quad \mu^{pm} = \frac{(1-\phi)\mu_{m0}}{1 + 6\phi\frac{\kappa_{m0} + 2\mu_{m0}}{9\kappa_{m0} + 8\mu_{m0}}} \quad (3)$$

Finally, the third step of homogenization allows the estimation of macroscopic elastic properties of heterogeneous materials by taking into account the effect of inclusions at the level 2:

$$\kappa^{hom} = \frac{\frac{(1-\rho)\kappa^{pm}}{3\kappa^{pm} + 4\mu^{pm}} + \frac{\rho\kappa_i}{3\kappa_i + 4\mu^{pm}}}{\frac{(1-\rho)}{3\kappa^{pm} + 4\mu^{pm}} + \frac{\rho}{3\kappa_i + 4\mu^{pm}}}; \quad \mu^{hom} = \frac{\frac{(1-\rho)\mu^{pm}}{\mu^{pm}(9\kappa^{pm} + 8\mu^{pm}) + 6\mu_s(\kappa^{pm} + 2\mu^{pm})} + \frac{\rho\mu_i}{\mu^{pm}(9\kappa^{pm} + 8\mu^{pm}) + 6\mu_i(\kappa^{pm} + 2\mu^{pm})}}{\frac{(1-\rho)}{\mu^{pm}(9\kappa^{pm} + 8\mu^{pm}) + 6\mu^{pm}(\kappa^{pm} + 2\mu^{pm})} + \frac{\rho}{\mu^{pm}(9\kappa^{pm} + 8\mu^{pm}) + 6\mu_i(\kappa^{pm} + 2\mu^{pm})}} \quad (4)$$

3. Formulation of plastic damage model

3.1. Macroscopic plastic yield criterion

It is assumed that the solid phase at the level 0 is a pressure sensitive material and obeys to the standard Drucker-Prager type yield criterion:

$$F^s = \tilde{\sigma}_d + T(\tilde{\sigma}_m - h) \leq 0 \quad (5)$$

in which $\tilde{\boldsymbol{\sigma}}$ denotes the stress tensor of the solid phase. $\tilde{\sigma}_m = \text{tr}\tilde{\boldsymbol{\sigma}}/3$ is the mean stress. $\tilde{\sigma}_d$ is the equivalent shear stress defined as $\tilde{\sigma}_d = \sqrt{\tilde{\boldsymbol{\sigma}}' : \tilde{\boldsymbol{\sigma}}'}$, with $\tilde{\boldsymbol{\sigma}}'$ being the deviatoric part of stress tensor. The parameter T denotes the frictional coefficient and h the yield stress under hydrostatic tension of the solid phase.

As illustrated in Figure 1, the porous matrix contains two populations of pores at two different scales. Therefore, two steps of non-linear homogenization are also needed to determine its effective plastic yield criterion. By using a modified secant method in [22], the elastic plastic yield criterion has been derived to consider the effects of small pore f and the dilatation of the solid phase at the level 0:

$$F^p = \frac{1 + 2f/3}{T^2} \tilde{\sigma}_d^2 + \left(\frac{3f}{2T^2} - 1\right) \tilde{\sigma}_m^2 + 2(1 - f)h\tilde{\sigma}_m - (1 - f)^2 h^2 \leq 0 \quad (6)$$

where $\tilde{\sigma}_d$ and $\tilde{\sigma}_m$ represent the equivalent shear stress and mean stress at the scale level 0. This criterion (6) explicitly depends on the small porosity f and the pressure sensitivity parameter T of the solid phase. Based on this criterion and again by using the modified secant method in [28], the effective plastic yield criterion can be obtained considering the influence of large pore ϕ at the level 1:

$$F^{mp} = A\sigma_d^2 + B\sigma_m^2 + C\sigma_m - D \leq 0 \quad (7)$$

with the following coefficients:

$$A = \frac{1 + 2f/3}{T^2} \left(\frac{6T^2 - 13f - 6}{4T^2 - 12f - 9} \phi + 1 \right), \quad B = \frac{3/2 + f}{T^2} \phi + \frac{3f}{2T^2} - 1 \quad (8)$$

$$C = 2(1 - f)(1 - \phi)h, \quad D = (1 - \phi)^2(1 - f)^2 h^2$$

In this criterion, σ_m and σ_d denote the mean and equivalent shear stresses at the scale level 1.

With the criterion (7) in hand, the objective here is now to determine an analytical macroscopic plastic yield criterion of composite material at the level 2 by considering the influence of rigid inclusions by a third step of homogenization. To this end, the modified secant method is again used and the main steps are presented below. By assuming an associated plastic flow rule, the local plastic strain rate of porous matrix is determined by:

$$\mathbf{d} = \lambda \frac{\partial F^{mp}}{\partial \boldsymbol{\sigma}} = \frac{1}{A} \frac{d_d}{2\sigma_d} (2A\boldsymbol{\sigma}' + \frac{2B\sigma_m}{3} \mathbf{1} + \frac{C}{3} \mathbf{1}) \quad (9)$$

in which $d_d = \sqrt{\mathbf{d}' : \mathbf{d}'}$ and $\mathbf{d}' = \mathbf{d} - d_m \mathbf{1}$. The mean plastic strain rate d_m is defined by:

$$d_m = \text{tr}\mathbf{d}/3 = \frac{1}{A} \frac{d_d}{2\sigma_d} \left[\frac{2\sigma_m}{3} B + \frac{C}{3} \right] \quad (10)$$

Accordingly the equivalent deviatoric strain rate is equal to:

$$\frac{d_d}{\sigma_d} = \sqrt{\frac{A^2 d_v^2 + AB d_d^2}{BD + \frac{C^2}{4}}} \quad (11)$$

Hence the support function defined as $\pi_{mp} = \boldsymbol{\sigma} : \mathbf{d}$ can be written in the following form:

$$\pi_{mp} = -\frac{C}{2B} d_v + \sqrt{\frac{4BD + C^2}{4AB}} \sqrt{\frac{A}{B} d_v^2 + d_d^2} \quad (12)$$

where $d_v = \text{tr} \mathbf{d} = 3d_m$ is the plastic volumetric strain rate in the porous matrix at the level 2.

The local stress tensor $\boldsymbol{\sigma}$ is derived from the support function π_{mp} by:

$$\boldsymbol{\sigma} = \frac{\partial \pi_{mp}}{\partial \mathbf{d}} = 2\mu^{mp} \mathbf{d}' + k^{mp} d_v \mathbf{1} + \sigma^p \mathbf{1} \quad (13)$$

with the following secant bulk and shear moduli and an isotropic pre-stress tensor:

$$k^{mp} = \frac{A}{B} \frac{N}{M}, \quad 2\mu^{mp} = \frac{N}{M}, \quad \sigma^p = -\frac{C}{2B} \quad (14)$$

$$M = \sqrt{\frac{A}{B} d_v^2 + d_d^2}, \quad N = \sqrt{\frac{4BD + C^2}{4AB}}$$

The secant moduli in (14) are non-uniform due to the non-uniform field of local strain rate \mathbf{d} inside the porous matrix. Following the work in [22], the values of secant moduli are calculated in terms of an effective strain rates d_d^{eff} and d_v^{eff} defined as follows:

$$d_v^{eff} = \sqrt{\langle d_v^2 \rangle_{\omega_m}}, \quad d_d^{eff} = \sqrt{\langle d_d^2 \rangle_{\omega_m}} \quad (15)$$

Therefore, the local stress-strain relations can be written as:

$$\boldsymbol{\sigma} = \mathbb{C}^{mp}(d_v^{eff}, d_d^{eff}) : \mathbf{d} + \sigma_{eq}^p \mathbf{1}; \quad \mathbb{C}^{mp}(d_v^{eff}, d_d^{eff}) = 3k_{eq}^{mp} \mathbb{J} + 2\mu_{eq}^{mp} \mathbb{K}; \quad \sigma_{eq}^p = \sigma^p \quad (16)$$

Owing to the assumption of plastically rigid inclusions, the macroscopic pre-stress simply reads $\Sigma^p = \sigma_{eq}^p$. Considering the effective free energy function of the composite with the form of:

$$W = \frac{1}{2} \mathbf{D} : \mathbb{C}^{hom} : \mathbf{D} + \Sigma^p \text{tr} \mathbf{D} \quad (17)$$

the corresponding state equations can be deduced as:

$$\Sigma_m = k^{hom}(\mathbf{D}_v + \Sigma^p); \quad \Sigma_d = 2\mu^{hom} D_d \quad (18)$$

Following the study of [50], the macroscopic free energy in the RVE is associated with the effective strain rate of porous matrix as follows:

$$\begin{aligned}\frac{1}{2}(1-\rho)d_v^{eff^2} &= \frac{1}{2}\frac{\partial k^{hom}}{\partial k_{eq}^{mp}}D_v^2 + \frac{\partial \mu^{hom}}{\partial k_{eq}^{mp}}D_d^2 \\ \frac{1}{2}(1-\rho)d_d^{eff^2} &= \frac{1}{2}\frac{\partial k^{hom}}{\partial \mu_{eq}^{mp}}D_v^2 + \frac{\partial k^{hom}}{\partial \mu_{eq}^{mp}}D_d^2\end{aligned}\quad (19)$$

By combining (15), (14), (18) and (19), one gets the following macroscopic plastic yield criterion of the composite material:

$$F = \frac{A + \frac{2B\rho}{3}}{1 + \frac{3\rho}{2} - \frac{5\rho}{6(\frac{A}{B}+1)}}\Sigma_d^2 + B\Sigma_m^2 + C\Sigma_m - (D + \frac{4BD + C^2}{6A}\rho) \leq 0 \quad (20)$$

A first assessment of this criterion can be made. One first considers the particular case of $f = 0$, $\phi = 0$ and $\rho = 0$. The macroscopic criterion reduces to the standard Drucker-Prager criterion of the solid phase at the scale level 0. When the material contains one population of pores either at the Level 0 or Level 1 ($\rho = 0$, and $f = 0$ or $\phi = 0$), one recovers the plastic criterion given by [22]. For the case of two populations of pores ($f \neq 0$, $\phi \neq 0$ and $\rho = 0$), this criterion is consistent with that proposed by [28] and given in (7). In Fig.2, one shows the yield surfaces of a material with two populations of pores but without inclusions. For a given total porosity of $\Gamma = 15\%$, different ratios of two porosities are considered ($f/\phi = 0, 0.2, 2, \infty$). It is seen that the compressive yield stress increases when the small porosity f decreases while the tensile yield stress is nearly insensitive to the ratio f/ϕ . In Fig.3, for the same value of total porosity $\Gamma = 15\%$, the volume fraction of inclusions is taken as $\rho = 20\%$. Again, four different values of the ratio f/ϕ are used and one confirms the result given in Fig.2 about the effect of f/ϕ on the yield stress. However, for the same value of total porosity, the macroscopic yield stresses obtained in Fig.3 are systematically smaller than those in Fig.2. Indeed, due to the presence of mineral inclusions, the volume of matrix phase is reduced and the values of local porosities f and ϕ are increased. This leads to the reduction of macroscopic yield stresses. Finally, for the given values of two porosities, the influence of inclusion volume fraction is studied and presented in Fig.4. It is observed that the increase of ρ mainly enhances the macroscopic yield stress for deviatoric loading paths.

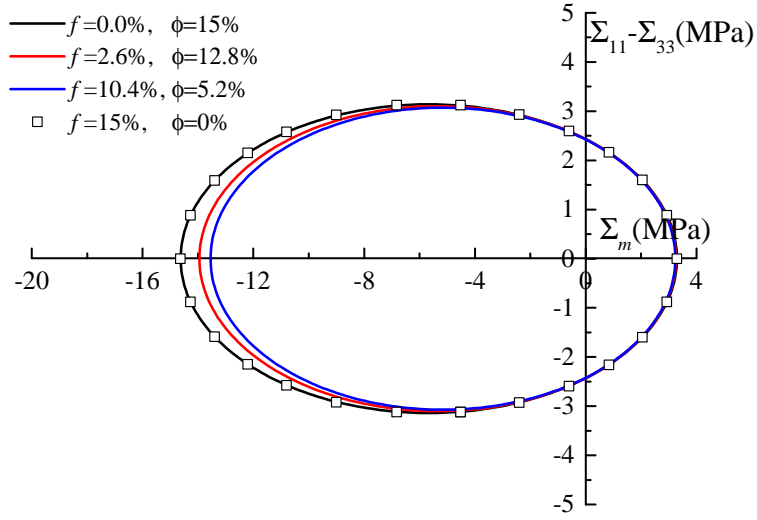


Figure 2: Macroscopic yield surfaces of materials with two populations of pores for different values of f/ϕ : $\Gamma = 15\%$, $\rho = 0.0\%$, $T = 0.3$, $h = 10MPa$

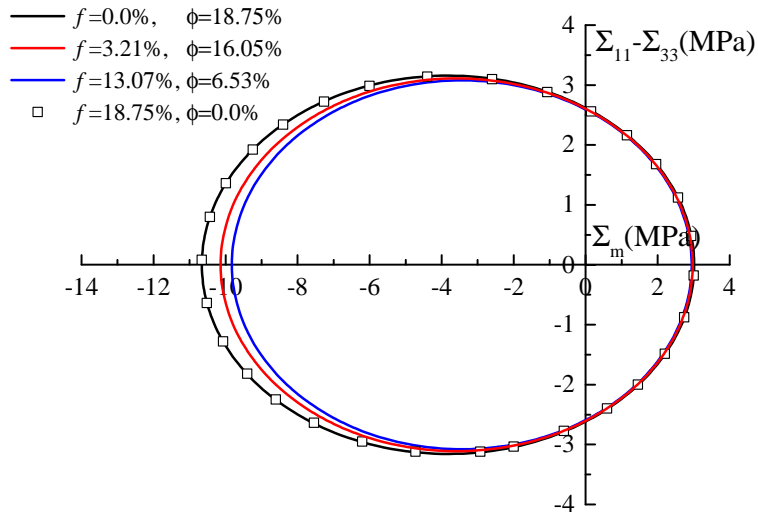


Figure 3: Macroscopic yield surfaces of materials with two populations of pores and mineral inclusions for different values of f/ϕ : $\Gamma = 15\%$, $\rho = 20\%$, $T = 0.3$, $h = 10MPa$

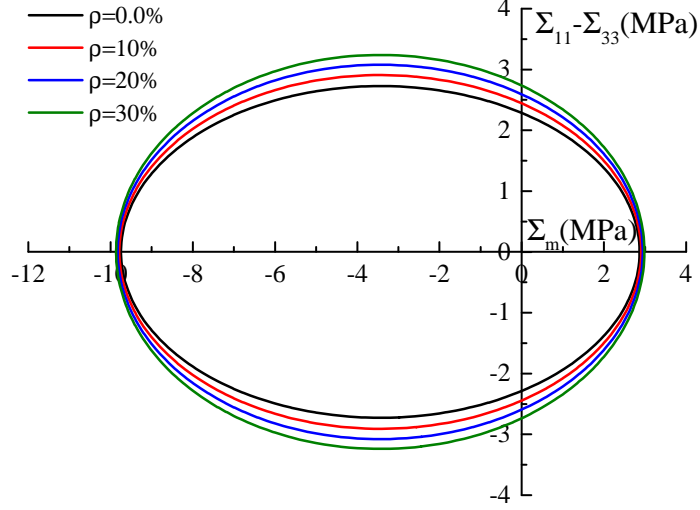


Figure 4: Macroscopic yield surfaces of materials with two populations of pores and inclusions for different inclusion volume fractions: $f = 13.07\%$, $\phi = 6.53\%$, $T = 0.3$, $h = 10MPa$

3.2. Evolution of porosity and hardening law

As defined above, the macroscopic plastic yield criterion is a function of two porosities. During a loading history, there is an evolution of those porosity. A decrease of porosities generally leads to an increase of yield stress and then a plastic hardening process, while an increase of porosities leads to a material softening. These phenomena have been observed in experimental studies of porous rocks [51, 52]. Therefore, it is needed to define the evolution laws for two porosities, allowing to describing the plastic hardening or softening. In this study, the nucleation of new pores is not considered. According to the first term of equation (1), the evolution rates of two porosities are given by:

$$\dot{f} = d\left(\frac{\omega_0}{\omega_s + \omega_0}\right) = (1 - f)\left(\frac{d\omega_s + d\omega_0}{\omega_s + \omega_0} - \frac{d\omega_s}{\omega_s}\right) \quad (21)$$

$$\dot{\phi} = d\left(\frac{\omega_1}{\omega_s + \omega_0 + \omega_1}\right) = (1 - \phi)\left(\frac{d\omega_m}{\omega_m} - \frac{d\omega_s + d\omega_0}{\omega_s + \omega_0}\right) \quad (22)$$

In these relations, $\frac{d\omega_s}{\omega_s}$ corresponds to the volumetric strain rate of solid phase (\tilde{d}_v) while $\frac{d\omega_s + d\omega_0}{\omega_s + \omega_0}$ to the volumetric strain rate of the porous matrix at the scale level 1 (\tilde{d}'_v). Further, $\frac{d\omega_m}{\omega_m}$ denotes the volumetric strain rate of the porous matrix at the scale level 2 (d_v). It is now assumed that the plastic strain of the solid phase is described by an associated flow rule with the Drucker-Prager type yield function defined by (5). The rate of plastic strain $\tilde{\mathbf{d}}$ is thus calculated by:

$$\tilde{\mathbf{d}} = \dot{\Lambda} \frac{\partial F^s}{\partial \tilde{\boldsymbol{\sigma}}}; \quad \tilde{\mathbf{d}}' = \dot{\Lambda} \frac{\tilde{\boldsymbol{\sigma}}'}{\tilde{\boldsymbol{\sigma}}'_d}; \quad \tilde{d}_m = \frac{1}{3} \dot{\Lambda} T \quad (23)$$

where $\tilde{\mathbf{d}}'$ is the deviatoric part of plastic strain rate tensor with $\tilde{\mathbf{d}} = \tilde{\mathbf{d}}' + \tilde{d}_m \boldsymbol{\delta}$. $\dot{\Lambda}$ is the non-negative plastic multiplier. The equivalent plastic strain rate $\dot{\epsilon}^p$ of the solid phase takes the following form:

$$\dot{\epsilon}^p = \sqrt{\tilde{\mathbf{d}}' : \tilde{\mathbf{d}}'} = \dot{\Lambda} \quad (24)$$

By applying the energy equivalence condition for upscaling methods [21], it is possible to associate the macroscopic plastic strain rate with that of the solid phase, that is:

$$\boldsymbol{\Sigma} : \mathbf{D}^p = \frac{1}{\omega} \int_{\omega_s} \tilde{\boldsymbol{\sigma}} : \tilde{\mathbf{d}} dV = \frac{1}{\omega} \int_{\omega_s} \dot{\epsilon}^p (\tilde{\sigma}_d + T \tilde{\sigma}_m) dV = (1 - \rho)(1 - \phi)(1 - f)Th \dot{\epsilon}^p \quad (25)$$

Therefore the equivalent strain rate of the solid phase $\dot{\epsilon}^p$ is calculated by:

$$\dot{\epsilon}^p = \frac{\boldsymbol{\Sigma} : \mathbf{D}^p}{(1 - \rho)(1 - \phi)(1 - f)Th} \quad (26)$$

On the other hand, the energy equivalence condition can also be applied to the porous matrix at the scale level 0 described by the yield criterion (6) so that:

$$\boldsymbol{\Sigma} : \mathbf{D}^p = \frac{1}{\omega} \int_{\omega_s + \omega_1} \tilde{\boldsymbol{\sigma}} : \tilde{\mathbf{d}} dV = \frac{1}{\omega} \int_{\omega_s + \omega_1} \frac{T^2}{1 + \frac{2}{3}f} \frac{\tilde{d}_d}{2\tilde{\sigma}_d} [(1 - f)^2 h^2 - 2(1 - f)h\tilde{\sigma}_m] dV \quad (27)$$

One can obtain:

$$\frac{\tilde{d}_d}{\tilde{\sigma}_d} = \frac{(1 + \frac{2f}{3})}{T^2} \frac{2\boldsymbol{\Sigma} : \mathbf{D}^p}{(1 - \rho)(1 - \phi)[(1 - f)^2 h^2 - 2(1 - f)h\tilde{\sigma}_m]} \quad (28)$$

$$\tilde{d}_v = \frac{(\frac{3f}{2T^2} - 1) \frac{2\Sigma_m}{(1-\rho)(1-\phi)} + 2(1-f)h}{(1-f)^2 h^2 - 2(1-f)h \frac{\Sigma_m}{(1-\rho)(1-\phi)}} \frac{\boldsymbol{\Sigma} : \mathbf{D}^p}{(1-\rho)(1-\phi)} \quad (29)$$

Further, according to the relations (23) and (24), the plastic volume strain rate of the solid phase is related to the equivalent plastic strain rate by $\tilde{d}_v = T \dot{\epsilon}^p$. Finally, the evolutions of porosities in (21) can be determined from the following kinematical compatibility conditions:

$$\dot{f} = (1 - f)(\tilde{d}_v - T \dot{\epsilon}^p) \quad (30)$$

$$\dot{\phi} = (1 - \phi) \left(\frac{tr \mathbf{D}^p}{1 - \rho} - \tilde{d}_v \right) \quad (31)$$

However, as it is well shown below, the evolutions of porosities alone cannot fully describe the plastic hardening process in porous rock-like materials. It is generally found that the local strength parameters of the solid phase such as frictional coefficient and cohesion evolve during plastic deformation process [53]. In this study, it is assumed that the frictional coefficient of the solid phase \bar{T} is a function of the equivalent plastic strain:

$$\bar{T} = T_m - (T_m - T_0)e^{-b\epsilon^p} \quad (32)$$

T_0 and T_m are the initial and asymptotic values of \bar{T} . The parameter b controls the plastic hardening rate.

3.3. Evolution of damage

The induced damage in rock-like materials is generally related to the evolution of their micro-structure [30, 54], and such an evolution is a time dependent process, which would be induced by mechanical or physical and chemical interactions, for instance, the microcracking [55], weathering-induced [56], chemical corrosion [57, 58] and so on. As a consequence, we introduce here a scalar damage variable ζ to represent the evolution state of micro-structure. It is assumed that there exists an asymptotic state of micro-structure evolution which is represented by a stationary value of the damage variable denoted as $\bar{\zeta} \in [0, 1]$. As for most chemical reaction processes, the rate of evolution is governed by the distance between the current value ζ and stationary values $\bar{\zeta}$. Thus one gets:

$$\dot{\zeta} = \gamma(\bar{\zeta} - \zeta), \quad \zeta \in [0, \bar{\zeta}] \quad (33)$$

where γ is a parameter that controls the rate of micro-structure evolution. By using Laplace transform and convolution theorem and taking $\zeta(0) = 0$, the damage variable ζ can be expressed in the following integral form:

$$\zeta(t) = \int_0^t \gamma \bar{\zeta}(\tau) e^{-\gamma(t-\tau)} d\tau \quad (34)$$

Due to the time-dependency of the stationary value $\bar{\zeta}(\tau)$, it is generally delicate to solve this integral equation. To this end, a simplified explicit scheme by using the rectangular integration rule has been proposed in [59]. In this study, that explicit scheme is modified by using a trapezoid rule to get a more accurate estimate. For a given time increment Δt_{n+1} , the variable ζ at the time step t_{n+1} is calculated by:

$$\zeta_{n+1} = \frac{\gamma}{2} \bar{\zeta}_{n+1} \Delta t_{n+1} + (\zeta_n + \frac{\gamma}{2} \bar{\zeta}_n \Delta t_{n+1}) e^{-\gamma \Delta t_{n+1}} \quad (35)$$

Further, in the present study, the stationary value of microstructure evolution $\bar{\zeta}$ is taken as the ratio of the current value of friction coefficient and its asymptotic value as defined in (32) so that:

$$\bar{\zeta} = \frac{\bar{T}}{T_m} \quad (36)$$

On the other hand, the evolution of micro-structure leads to degradation of both elastic and plastic properties of materials. It is here assumed that the micro-structure degradation mainly occurs in the solid phase which mainly induced by the cracking behavior during the deformation process. From the point of micromechanics, sliding wing cracks seem to be the principal propagation mode of microcracks under compressive stresses [60]. Due to roughness of crack surfaces in geomaterials, crack sliding may induce an associated aperture which is

the origin of volumetric dilatancy in these materials [61]. Therefore, a direct relationship is established to consider the influence of microcracking or frictional sliding damage on the macroscopic mechanical behavior though the degradation of elastic and friction parameters of the solid phase. Similar consideration can also be found in [62, 63]. Therefore, the elastic properties and the frictional coefficient are functions of the damage variable ζ . For the sake of simplicity, the following linear relations are adopted:

$$k_d = (1 - \alpha\zeta)k^s, \quad \mu_d = (1 - \alpha\zeta)\mu^s \quad (37)$$

and

$$T = (1 - \alpha\zeta)\bar{T} \quad (38)$$

where α is a parameter controlling the degradation rate of elastic and plastic properties.

3.4. Macroscopic plastic damage constitutive relations

By including plastic deformation and damage evolution, the incremental macroscopic constitutive relations can be expressed as:

$$d\boldsymbol{\Sigma} = \mathbb{C}_d^{hom} : (\mathbf{D} - \mathbf{D}^p) + \frac{\partial \mathbb{C}_d^{hom}}{\partial \zeta} : (\tilde{\mathbf{D}} - \tilde{\mathbf{D}}^p) d\zeta \quad (39)$$

where $\tilde{\mathbf{D}}$ and $\tilde{\mathbf{D}}^p$ are the accumulated total strain and plastic strain tensors. The accumulated elastic strain tensor is given by $\tilde{\mathbf{D}}^e = \tilde{\mathbf{D}} - \tilde{\mathbf{D}}^p$. The fourth order tensor \mathbb{C}_d^{hom} denotes the current macroscopic elastic stiffness of damage material with respect to damage variable ζ . By adopting an associated flow rule, the macroscopic plastic strain rate is given by:

$$\mathbf{D}^p = d\lambda \frac{\partial \mathbf{F}}{\partial \boldsymbol{\Sigma}} \quad (40)$$

The plastic multiplier $d\lambda$ is determined by the consistency condition:

$$d\mathbf{F} = \frac{\partial \mathbf{F}}{\partial \boldsymbol{\Sigma}} : d\boldsymbol{\Sigma} + \frac{\partial \mathbf{F}}{\partial f} df + \frac{\partial \mathbf{F}}{\partial \phi} d\phi + \frac{\partial \mathbf{F}}{\partial T} \left(\frac{\partial T}{\partial \epsilon^p} : d\epsilon^p + \frac{\partial T}{\partial \zeta} d\zeta \right) = 0 \quad (41)$$

Substituting (26), (29), (30), (31), (39) and (40) for (41), one obtains:

$$d\lambda = \frac{\frac{\partial \mathbf{F}}{\partial \boldsymbol{\Sigma}} : \mathbb{C}_d^{hom} : \mathbf{D} + \frac{\partial \mathbf{F}}{\partial \boldsymbol{\Sigma}} : \frac{\partial \mathbb{C}_d^{hom}}{\partial \zeta} : \tilde{\mathbf{D}}^e d\zeta + \frac{\partial \mathbf{F}}{\partial T} \frac{\partial T}{\partial \zeta} d\zeta}{\frac{\partial \mathbf{F}}{\partial \boldsymbol{\Sigma}} : \mathbb{C}^{hom} : \frac{\partial \mathbf{F}}{\partial \boldsymbol{\Sigma}} - \frac{\partial \mathbf{F}}{\partial f} (1-f) [\tilde{\mathbf{d}}_f - T \tilde{\mathbf{d}}_p] - \frac{\partial \mathbf{F}}{\partial \phi} (1-\phi) \left(\frac{\frac{\partial \mathbf{F}}{\partial \Sigma_m}}{1-\rho} - \tilde{\mathbf{d}}_f \right) - \frac{\partial \mathbf{F}}{\partial T} \frac{\partial T}{\partial \epsilon^p} \tilde{\mathbf{d}}_p} \quad (42)$$

with

$$\tilde{\mathbf{d}}_f = \frac{\left(\frac{3f}{2T^2} - 1 \right) \frac{2\Sigma_m}{(1-\rho)(1-\phi)} + 2(1-f)h}{(1-f)^2 h^2 - 2(1-f)h \frac{\Sigma_m}{(1-\rho)(1-\phi)}} \boldsymbol{\Sigma} : \frac{\partial \mathbf{F}}{\partial \boldsymbol{\Sigma}} \quad (43)$$

$$\tilde{\mathbf{d}}_p = \frac{\boldsymbol{\Sigma} : \frac{\partial \mathbf{F}}{\partial \boldsymbol{\Sigma}}}{(1-\rho)(1-\phi)(1-f)Th} \quad (44)$$

3.5. Numerical implementation

With these relations in hand, the proposed plastic damage constitutive model can be implemented in a standard finite element code by using an appropriate return-mapping scheme. In the present work, only instantaneous mechanical problems are taken into account. Then the whole loading process is divided into a limit numbers of steps. The integration algorithm at time interval $[t_{k-1}, t_k]$ can be summarized as follows:

- (1) At the end of the time step t_{k-1} , the current values of stress and strain as well as those of internal variables such as accumulated equivalent plastic strain and damage are known: $\boldsymbol{\Sigma}_{k-1}$, $\tilde{\mathbf{D}}_{k-1}$, $\boldsymbol{\epsilon}_{k-1}^p$, $\bar{\zeta}_{k-1}$, ζ_{k-1} , f_{k-1} , ϕ_{k-1} , T_{k-1} .
- (2) Given an strain increment $\Delta\tilde{\mathbf{D}}$ in time increment Δt_k , a new trial stress can be determined by $\boldsymbol{\Sigma}_{k,0}^{tr} = \boldsymbol{\Sigma}_{k-1}^{tr} + \Delta\boldsymbol{\Sigma}_k$ at time step t_k , with $t_k = t_{k-1} + \Delta t_k$.
- (3) Set j as the loop iterate step of return-mapping scheme, and impose the initial values of $\bar{\zeta}_{k,0} = \bar{\zeta}_{k-1}$, $\boldsymbol{\epsilon}_{k,0}^p = \boldsymbol{\epsilon}_{k-1}^p$, $f_{k,0} = f_{k-1}$, $\phi_{k,0} = \phi_{k-1}$, $T_{k,0} = T_{k-1}$.
- (4) Using Eq.(35) to calculate the damage variable $\zeta_{k,0}$ at initial iterative step .
- (5) Calculate the plastic criterion $F(\boldsymbol{\Sigma}_{k,j}^{tr}, f_{k,j}, \phi_{k-1}, \boldsymbol{\epsilon}_{k,j}^p, \zeta_{k,j})$ in Eq.(20). If $F(\boldsymbol{\Sigma}_{k,j}^{tr}, f_{k,j}, \phi_{k,j}, \boldsymbol{\epsilon}_{k,j}^p, \zeta_{k,j}) \leq 0$, it has $\boldsymbol{\Sigma}_k = \boldsymbol{\Sigma}_{k,j}^{tr}$, then goto step (9).
- (6) If $F(\boldsymbol{\Sigma}_{k,j}^{tr}, f_{k,j}, \phi_{k-1}, \boldsymbol{\epsilon}_{k,j}^p, \zeta_{k,j}) > 0$, start the loop to determine the multiplier though Eq.(42), then calculate the plastic strain $\tilde{\mathbf{D}}_{k,j}$ and equivalent plastic strain rate $\dot{\boldsymbol{\epsilon}}_{k,j}^p$ by Eq.(26).
- (7) Update the internal variables $\boldsymbol{\epsilon}_{k,j+1}^p$, $\bar{\zeta}_{k,j+1}$, $f_{k,j+1}$, $\phi_{k,j+1}$, $T_{k,j+1}$, the stress tensor $\boldsymbol{\Sigma}_{k,j+1}$ and damage $\zeta_{k,j+1}$.
- (8) Set $j = j + 1$, then goto step (5) until $F(\boldsymbol{\Sigma}_{k,j}^{tr}, f_{k,j}, \phi_{k-1}, \boldsymbol{\epsilon}_{k,j}^p, \zeta_{k,j}) \leq 0$ and exit the loop.
- (9) One can get the internal variables $\bar{\zeta}_k = \bar{\zeta}_{k,j+1}$, $\boldsymbol{\epsilon}_k^p = \boldsymbol{\epsilon}_{k,j+1}^p$, $f_k = f_{k,j+1}$, $\phi_k = \phi_{k,j+1}$, $T_k = T_{k,j+1}$, the stress tensor $\boldsymbol{\Sigma}_k = \boldsymbol{\Sigma}_{k,j+1}$ and the damage variable $\zeta_k = \zeta_{k,j+1}$ at time step t_k . Then enter the next loading time step t_{k+1} .

Though above integration algorithm, the plastic and damage behavior of multi-scale rock-like materials can be well determined. This will be presented and discussed in detail in the following section.

4. Numerical assessment of the proposed model

4.1. Assessment of macroscopic yield criterion

The accuracy of the analytical macroscopic yield criterion (20) is first assessed by comparing the predicted yield stresses with those obtained by the Fast Fourier Transform (FFT) based numerical homogenization method. The basic principle and numerical implementation of FFT-based method can be found in [64, 65] for metal materials and in [9, 10] for rock-like materials. Due to the fact that the effects of inclusion size, distributions and shape have very slightly influences on the plastic yield stress [9], for simplicity, the cubic unit cell with one centered spherical inclusion embedded in a double porous matrix is adopted for all the FFT-based simulations. It is assumed that the double porous matrix obeys the plastic yield criterion in Eq.(7) with a perfect elasto-plastic behavior. This criterion can well describe the homogenized mechanical properties of scale 0 and scale 1 for materials with two populations of pores embedded in a DP type matrix. Then the inclusion is assumed to be elastic, thus the macroscopic behavior can be determined by using the FFT-based homogenization method. Within the FFT-based framework and the analytical homogenization criterion, we show the results of yield stress predicted by these two methods for different values of inclusion volume fraction and porosity in Fig.5 and Fig.6. As shown in these figures, for the given values of two porosities, the increase of inclusion volume fraction mainly enhances the yield strength with low and middle triaxiality. For a given value of inclusion volume fraction, the macroscopic yield strength is reduced by the increase of one of both porosities for the whole loading domain including hydrostatic tension and compression. For all the cases shown, there is a very good concordance between the analytical predictions and numerical results.

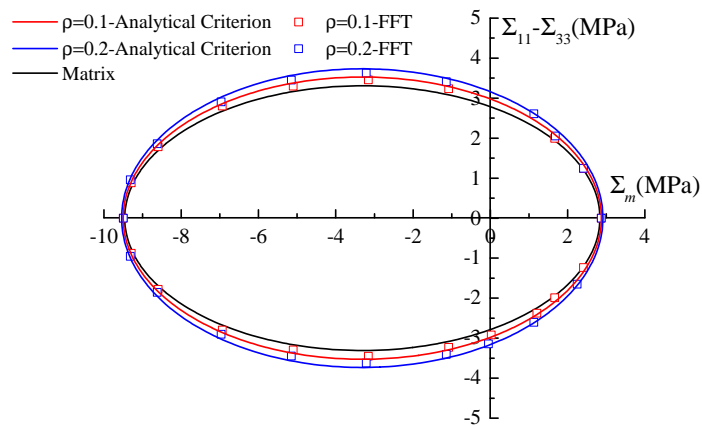


Figure 5: Comparison of macroscopic yield strength between the analytical predictions and FFT-based numerical results for different values of inclusion volume fraction: $f = 0.1, \phi = 0.1, T = 0.3, h = 20$ MPa

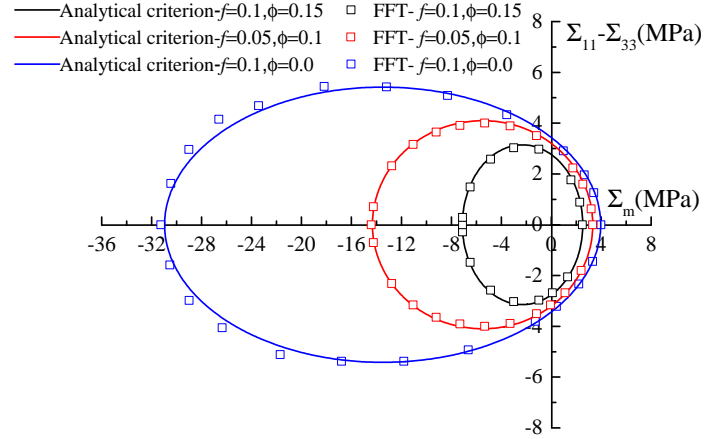


Figure 6: Comparison of macroscopic yield strength between the analytical predictions and FFT-based numerical results for different values of porosities: $\rho = 0.1, T = 0.3, h = 20$ MPa

4.2. Assessment of macroscopic response

By using the plastic hardening and damage laws proposed above, the macroscopic mechanical response of heterogeneous materials is here assessed. As an advantage of the micro-mechanics based model, it is possible to explicitly investigate the influences of micro-structural parameters on the macroscopic response, for instance the small porosity, the large porosity and the volume fraction of mineral inclusions. For this purpose, a series of numerical simulations are performed under uniaxial compression loading. The set of basic parameters used in the simulations are given in Table 1.

In Fig.7, we show the macroscopic axial and lateral strains versus the differential stress for four different values of the ratio between the small and large porosities ($f/\phi = 0, 0.2, 2, \infty$) but with the same total porosity of $\Gamma = 15\%$ and without mineral inclusions $\rho = 0$. It is found that the peak differential stress is reduced by the increase of the small porosity. It seems that the macroscopic strength is more sensitive to the small porosity at the scale level 0 than to the large one at the level 1. The same kind of results are obtained in the composite material containing mineral inclusions as shown in Fig.8 for a volume fraction of $\rho = 20\%$. Finally, the numerical results for different values of mineral inclusions fraction are shown in Fig.9. It is clear that the macroscopic peak strength is significantly reinforced by the presence of rigid inclusions at the scale level 2. On the other hand, the material softening behavior due to the growth of micro-cracks in the post-peak regime is also correctly described by the proposed model.

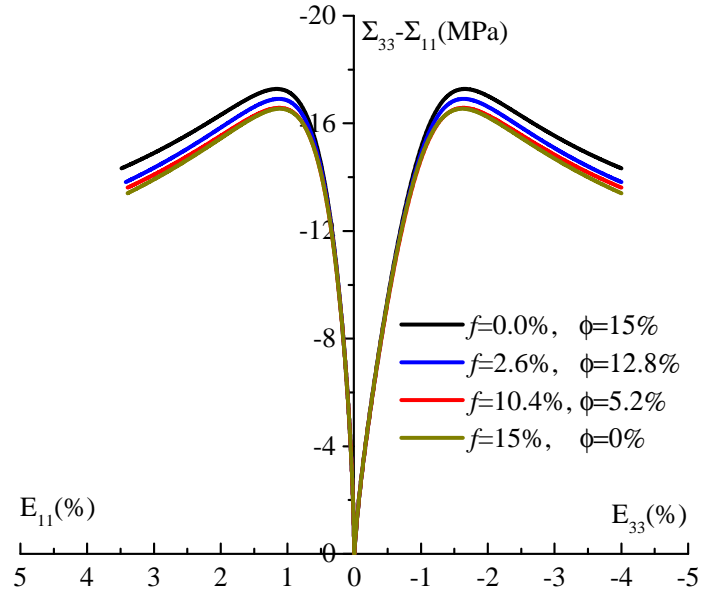


Figure 7: Macroscopic stress-strain curves uniaxial compression test for different values of porosity ratio f/ϕ without mineral inclusions: $\Gamma = 15\%$, $\rho = 0.0\%$

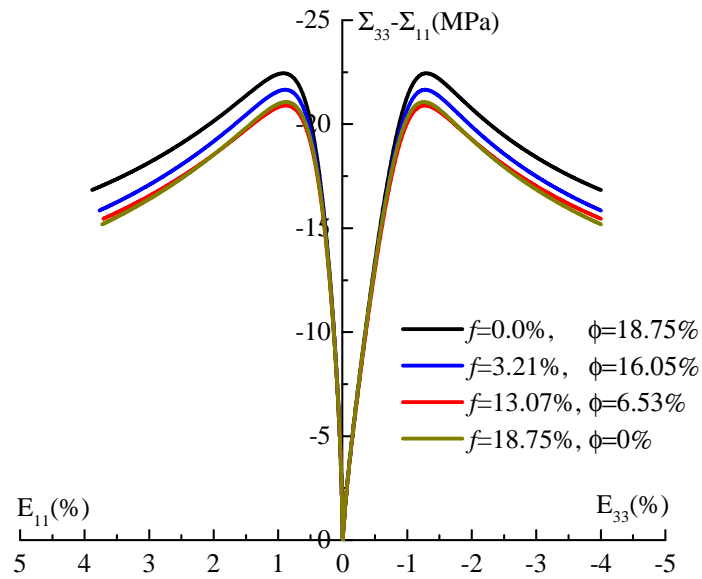


Figure 8: Macroscopic stress-strain curves in uniaxial compression test for different values of porosity ratio f/ϕ with the presence of mineral inclusions: $\Gamma = 15\%$, $\rho = 20\%$

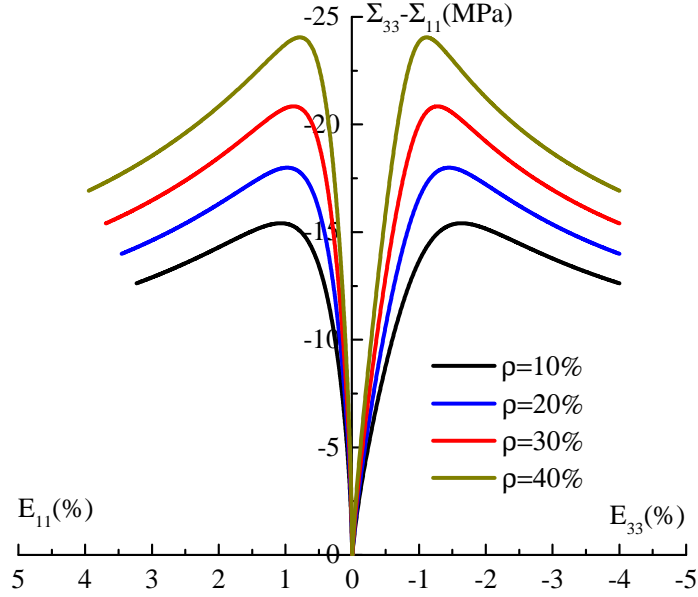


Figure 9: Macroscopic stress-strain curves in uniaxial compression test for different values of inclusions fraction and fixed porosities: $f = 10\%$, $\phi = 10\%$

5. Experimental verification with laboratory tests

5.1. Callovo-Oxfordian claystone

In this section, the proposed model is applied to study the mechanical behavior of the Callovo-Oxfordian claystone (COx). As mentioned above, this rock has been widely investigated as a potential geological barrier for underground disposal of radioactive waste in France [66]. This material is composed of 40 to 50% of clay minerals, 20 to 27% of quartz and 23 to 25% of calcite [12]. The mechanical behavior of the COx claystone was strongly influenced by the mineral compositions, water content and temperature [67, 68, 69]. The average total porosity is about 11.04-13.84%. The quasi totality of pores are distributed inside the clay minerals and their size ranges from 1 nm to 100 μm across different scales. According to [12] and as a first approximation, two populations of pores are here considered, respectively at the scale levels 0 and 1. A critical size of the pores nearly 8 nm is adopted by [70] to distinguish the small pores (corresponding to the porosity at level 0) from the large pores (corresponding to the porosity at level 1) for the claystone. As a consequence, the large pores has an average pore size 28 ± 5 nm. The rest pores are configured at a smaller scale. Therefore, the majority of pores are embedded at the level 1 and represent 95% of all pores. Only 5% of pores are at the level 0 according to the pore size distribution curves as presented in [70]. In addition, as indicated by [71], the size of the grains is usually larger

than $4 \mu\text{m}$ with a mean around $10\text{-}20 \mu\text{ m}$. It is much larger than the pores in clay matrix. Therefore, the inclusions are assumed to be embedded at level 2. Thus these three-scale characters can be well described by the proposed model in this work.

As the elastic properties of quartz and calcite are quite close to each other, for the sake of simplicity, they are merged into a single inclusion phase as used in some previous studies [19]. The elastic properties of the inclusion phase are taken as the average values of the ones of quartz and calcite as $E_i = 98 \text{ GPa}$ and $\nu_i = 0.15$. The plastic and damage parameters are calibrated by a numerical optimization method as indicated in [28]. The set of parameters are iteratively fitted from macroscopic responses obtained in a laboratory test with known mineralogical compositions. These parameters are then used in simulations of other tests with different mineral compositions. The parameters used in this study for the studied claystone are given in Table 1.

Table 1: Typical values of parameters for the COx claystone

Parameter	Clay matrix	Inclusion
Elastic parameters	$E_s = 5.027 \text{ GPa}$, $\nu_s = 0.33$	$E_i = 98 \text{ GPa}$, $\nu_i = 0.15$
Plastic parameters	$T_0 = 0.0001$, $T_m = 0.84$, $b = 170$, $h = 34 \text{ MPa}$	
Damage parameters	$\alpha = 0.34$, $\gamma = 4 \times 10^{-4}$	
Porosity	$f_1 = 1.6\%$, $\phi = 23.75\%$	

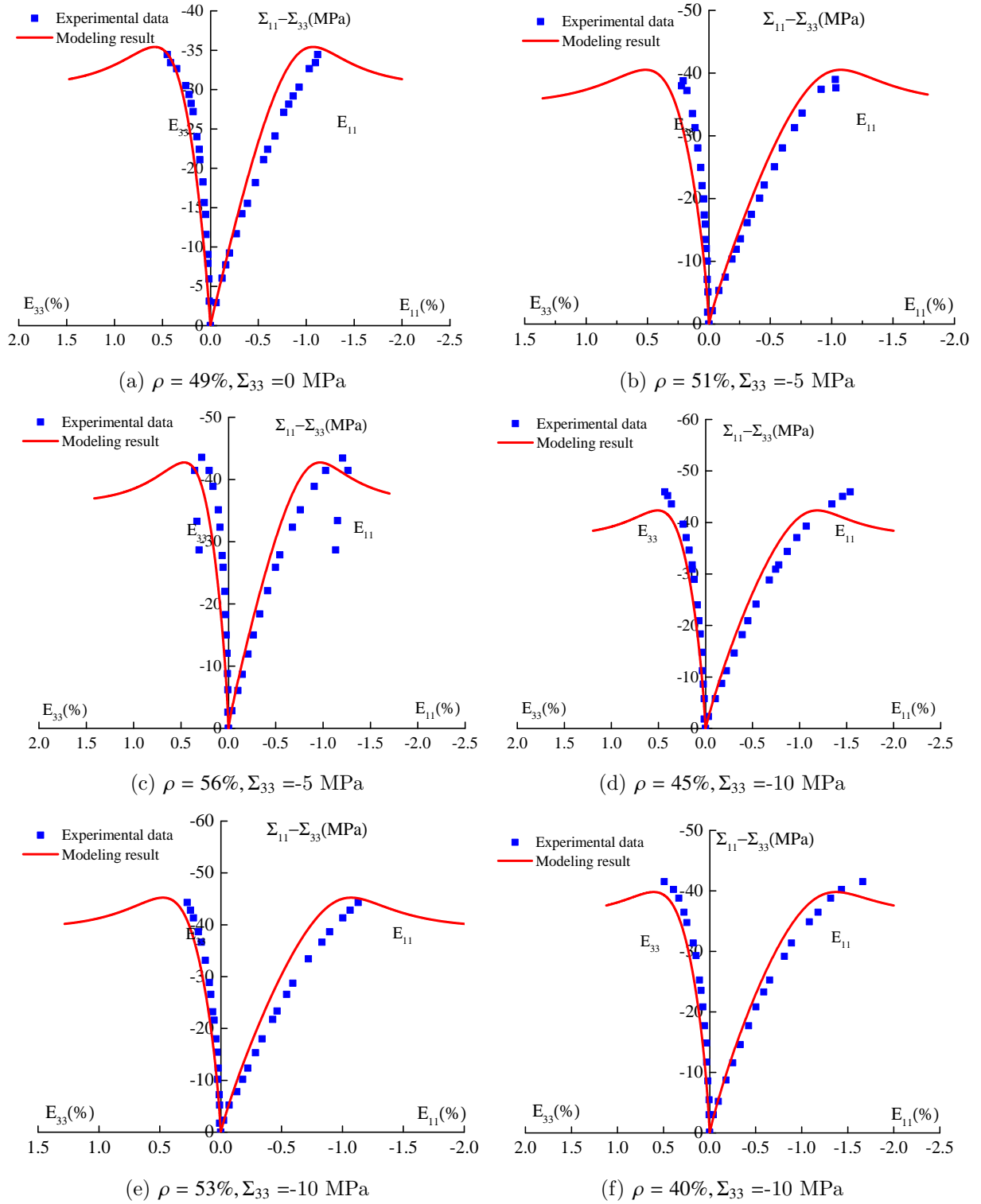


Figure 10: Comparison of stress-strain curves between numerical results and experimental data: $f = 1.6\%$, $\phi = 23.75\%$ under different confining pressure

In Fig.10, one presents the comparisons of macroscopic stress-strain curves between numerical results and experimental data for triaxial compression tests with different confining pressures ($\Sigma_{33} = 0, -5, -10$ MPa) and performed on samples with different micro-structural compositions. For these tests, the applied axial strain rate was $2 \times 10^{-6} s^{-1}$. From these comparisons, it is seen that the proposed model well reproduces the mechanical behavior for all the tests. On the other hand, by taking into account the damage evolution in the present model, the post-peak behavior of the COx claystone is properly described. This is a significant improvement of previous micro-mechanics based models for this kind of rocks, for instance the modified incremental model proposed in [28].

5.2. Vaca Muerta shale rock

The shale rock is an organic rich fine-grained sedimentary rock, containing complex mineralogy and pore networks [72]. Two and three dimensional microscopic observations have revealed that three representative length scales should be taken into account, as illustrated in Fig.11. At the scale level 2, different kinds of minerals, including quartz, carbonate, feldspar, kerogen and pyrite are embedded in a matrix phase. The size of those mineral grains varies from a few hundred micrometers to one or two millimeters [73]. At the scale level 1, fine calcite and kerogen grains are distributed in a solid phase. The majority of pores are found at the scale level 0 and their size is of a few nanometers [74, 72]. Therefore, by assuming again that all mineral inclusions and pores are of spherical form, the three-scale representative elementary volume (REV) of the shale is presented in Fig.11. For convenience, the porosity at the level 0 is denoted by f . The volume fraction of fine kerogen and calcite grains at the level 1 are defined as f_5 and f_6 . At the level 2, the big calcite is denoted by f_1 , the quartz/albite by f_2 , the pyrite by f_3 and the kerogen grains by f_4 .

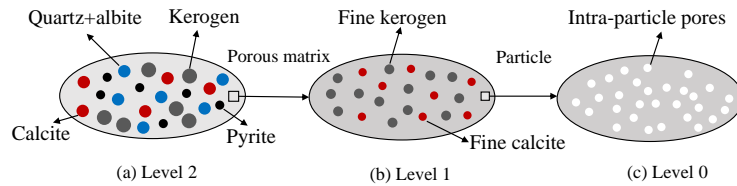


Figure 11: Representative volume element of an organic rich shale shale

As for the COx claystone, a linear elastic behavior is assumed for all the mineral inclusions. This is a strong assumption for the kerogen particles for the sake of simplicity. A more appropriate behavior should be considered in future studies. On the other hand, as a difference with the COx claystone, the elastic properties of different phases of inclusions at

the scales levels 1 and 2 can be significantly different. In order to keep an analytical homogenized model for both the elastic and plastic modeling. A simplified method is adopted. The inclusions at the scale level 1 (or 2) are first homogenized into an equivalent inclusion phase by using a self-consistent scheme [75]. The equivalent inclusion phase is then embedded into the porous matrix at the level 1 (or 2). Finally, the effective elastic properties of inclusion reinforced composite at the level 1 (or 2) shown in Fig. 11 are determined by using the Mori-Tanaka scheme given in (4) by replacing the elastic properties of inclusion phase κ_i and μ_i by those of the equivalent inclusion phase κ_i^{eq} and μ_i^{eq} , which are determined by the following iterative calculation:

$$\kappa_i^{eq} = \sum_{r=0}^N f_r \frac{\kappa_r(3\kappa_i^{eq} + 4\mu_i^{eq})}{3\kappa_r + 4\mu_i^{eq}}; \quad \mu_i^{eq} = \sum_{r=0}^N f_r \frac{5\mu_r\mu_i^{eq}(3\kappa_i^{eq} + 4\mu_i^{eq})}{\mu_i^{eq}(9\kappa_i^{eq} + 8\mu_i^{eq}) + 6\mu_r(\kappa_i^{eq} + 2\mu_i^{eq})} \quad (45)$$

f_r is the volume fraction of the r -th inclusion phase and κ_r and μ_r denote its elastic moduli. The elastic properties of the mineral inclusions are taken from literature [74, 72] and listed in Table 2.

Table 2: Typical values of parameters for the model

Mineral	Elastic modulus(GPa)	Poisson
Quartz/albite	95.5	0.155
Pyrite	311	0.15
Kerogen	2	0.25
Calcite	95	0.27
Clay	5	0.27

Due to the presence of small inclusions at the scale level 1 instead of pores, the plastic model is also adapted for the shale. By making two steps of homogenization with the modified secant method as presented in [19], the macroscopic plastic yield criterion keeps the same form as that given in (20). However, the coefficients in that equation are changed by taking into account of the small inclusion volume fraction at the scale level 1 ($\rho_s = f_5 + f_6$):

$$A = \frac{\frac{1+2f/3}{T^2} + \frac{2}{3}\rho_s(\frac{3f}{2T^2} - 1)}{\frac{6T^2-13f-6}{4T^2-12f-9}\rho_s + 1}, \quad B = \frac{3f}{2T^2} - 1 \quad (46)$$

$$C = 2(1-f)h, \quad D = \frac{3+2f+3f\rho_s}{3+2f}(1-f)^2h^2$$

In the present case, only one population of pores exists at the level 0. By making the similar derivation as that presented above for two populations of pores, its evolution is described

by:

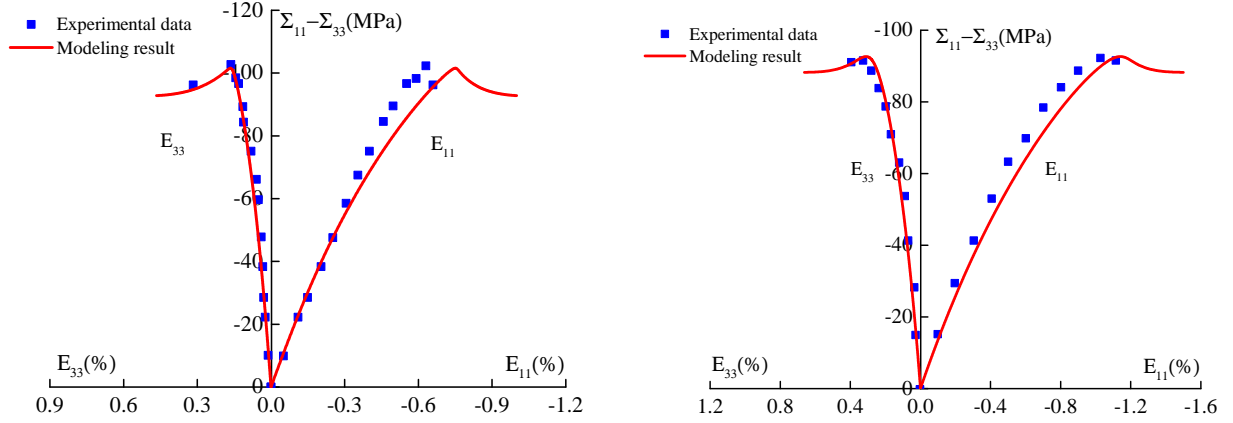
$$\dot{f} = (1 - f) \left(\frac{\text{tr} \mathbf{D}^p}{(1 - \rho)(1 - \rho_s)} - T \dot{\epsilon}^p \right) \quad (47)$$

The damage evolution law remains unchanged. The modified elastic-plastic damage model can now be applied to materials with two populations of inclusions at two different scales. It is here applied to describe the mechanical behavior of the Vaca Muerta shale rock. Again, a series of triaxial compression tests have been performed with different mineralogical compositions and confining pressures. The applied axial strain rate was 10^{-6}s^{-1} . The set of parameters used for the solid phase is given in Table 3:

Table 3: Typical values of parameters for the solid phase of Vaca Muerta shale

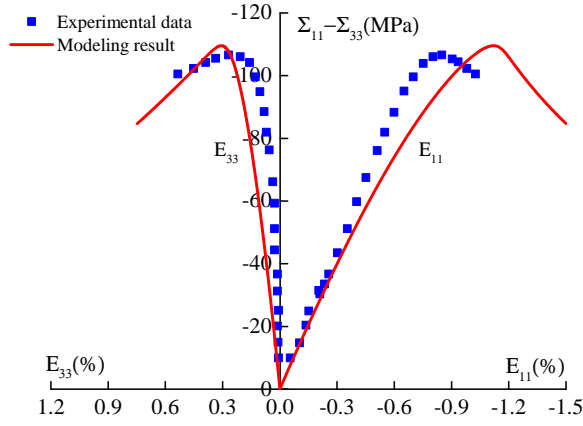
Parameter	Clay matrix
Elastic parameters	$E_s = 5.027 \text{ GPa}$, $\nu_s = 0.33$
Plastic parameters	$T_0 = 0.0001$, $T_m = 0.75$, $b = 600$, $h = 68 \text{ MPa}$
Damage parameters	$\alpha = 0.4$, $\gamma = 6 \times 10^{-4}$

In Fig.12, we present the comparisons of macroscopic stress-strain curves between the numerical results and experimental data. In a general way, a good agreement is found. The proposed micro-mechanics based model is able to well describe the dependency of macroscopic behavior of shale rocks on micro-structural compositions. Further, the post-peak behavior due to damage evolution is also correctly reproduced.



(a) $\Sigma_{33} = -2$ MPa: $f_1 = 40\%$, $f_2 = 30\%$, $f_4 = 25.7\%$, $f_6 = 5\%$, $f = 5\%$

(b) $\Sigma_{33} = -10$ MPa: $f_1 = 42.3\%$, $f_2 = 21.5\%$, $f_3 = 1.73\%$, $f_5 = 23\%$, $f = 9.4\%$



(c) $\Sigma_{33} = -10$ MPa: $f_1 = 24.15\%$, $f_2 = 17.3\%$, $f_4 = 26.4\%$, $f_6 = 25\%$, $f = 8\%$

Figure 12: Comparison of stress-strain curves of shale rock between numerical results and experimental data under different confining pressure

6. Concluding remarks

In this work, a unified analytical macroscopic yield criterion has been developed for a class of rock-like materials containing pores and inclusions at three different scales from a rigorous homogenization method. This criterion can cover a large range of rock-like materials with different multi-scale characters. The accuracy of the criterion was well verified by the numerical results issued from FFT-based simulations. Together with the plastic hardening and a damage evolution law acting on the solid phase of micro-structure, a new micromechanical-based plastic damage model is established and explicitly considers both the effects of pores and mineral inclusions at different scales. Then it was successfully applied

to predict the mechanical behaviors of two typical heterogeneous rocks, the COx claystone with two populations of pores and one family of inclusions, and the Vaca Muerta shale rock containing two populations of inclusions and one family of pores. The modeling results reveal a good agreement with the experimental data of triaxial compression test. It is found that the proposed model quantitatively well reproduce the main features of those materials responses. In future studies, time-dependent behaviors related to the damage evolution on visco-plastic deformation of solid phase as well as viscosity of kerogen particles should be taken into account.

Acknowledgements:

This study was supported by the the National Key RD Program of China (Grant No. 2017YFC1501101), Programme B18019 of Discipline Expertise to Universities MOE & MST and the National Natural Science Foundation of China (Grant No. 11672343).

References

- [1] A. Tuğrul, I. Zarif, Correlation of mineralogical and textural characteristics with engineering properties of selected granitic rocks from turkey, *Engineering Geology* 51 (4) (1999) 303–317.
- [2] R. S. Tandon, V. Gupta, The control of mineral constituents and textural characteristics on the petro-physical & mechanical (pm) properties of different rocks of the himalaya, *Engineering Geology* 153 (2013) 125–143.
- [3] Ö. Ündül, Assessment of mineralogical and petrographic factors affecting petro-physical properties, strength and cracking processes of volcanic rocks, *Engineering Geology* 210 (2016) 10–22.
- [4] Z. Liu, J. Shao, S. Xie, N. Conil, W. Zha, Effects of relative humidity and mineral compositions on creep deformation and failure of a claystone under compression, *International Journal of Rock Mechanics and Mining Sciences* 103 (2018) 68 – 76.
- [5] Q.-X. Meng, H.-L. Wang, W.-Y. Xu, Y.-L. Chen, Numerical homogenization study on the effects of columnar jointed structure on the mechanical properties of rock mass, *International Journal of Rock Mechanics and Mining Sciences* 124 (2019) 104127.
- [6] Q. Meng, H. Wang, W. Xu, M. Cai, J. Xu, Q. Zhang, Multiscale strength reduction method for heterogeneous slope using hierarchical fem/dem modeling, *Computers and Geotechnics* 115 (2019) 103164.
- [7] P. Baud, T.-f. Wong, W. Zhu, Effects of porosity and crack density on the compressive strength of rocks, *International Journal of Rock Mechanics and Mining Sciences* 67 (2014) 202–211.
- [8] M. Heidari, G. Khanlari, M. Torabi-Kaveh, S. Kargarian, S. Saneie, Effect of porosity on rock brittleness, *Rock mechanics and rock engineering* 47 (2) (2014) 785–790.
- [9] Y. Cao, W. Shen, N. Burlion, J. Shao, Effects of inclusions and pores on plastic and viscoplastic deformation of rock-like materials, *International Journal of Plasticity* 108 (2018) 107 – 124.
- [10] Y. Cao, W. Shen, J. Shao, N. Burlion, Influences of micro-pores and meso-pores on elastic and plastic properties of porous materials, *European Journal of Mechanics - A/Solids* 72 (2018) 407 – 423.

- [11] W. Shen, J. Shao, Z. Liu, A. Oueslati, G. De Saxcé, Evaluation and improvement of macroscopic yield criteria of porous media having a drucker-prager matrix, *International Journal of Plasticity* (2019) 102609.
- [12] J.-C. Robinet, Minéralogie, porosité et diffusion des solutés dans l’argilite du callovo-oxfordien de bure (meuse, haute-marne, france) de l’échelle centimétrique à micrométrique, Ph.D. thesis, Poitiers (2008).
- [13] J.-C. Robinet, P. Sardini, D. Coelho, J.-C. Parneix, D. Prêt, S. Sammartino, E. Boller, S. Altmann, Effects of mineral distribution at mesoscopic scale on solute diffusion in a clay-rich rock: Example of the callovo-oxfordian mudstone (bure, france), *Water Resources Research* 48 (5) (2012).
- [14] S. Abedi, M. Slim, R. Hofmann, T. Bryndzia, F. Ulm, Nanochemo-mechanical signature of organic-rich shales: a coupled indentation-edx analysis, *Acta Geotechnica* 11 (2016) 559–572.
- [15] S. Cariou, L. Dormieux, F. Skoczylas, An original constitutive law for callovo-oxfordian argillite, a two-scale double-porosity material, *Applied Clay Science* 80 (2013) 18–30.
- [16] M. Gărăjeu, P. Suquet, Effective properties of porous ideally plastic or viscoplastic materials containing rigid particles, *Journal of the Mechanics and Physics of Solids* 45 (6) (1997) 873–902.
- [17] P.-G. Vincent, Y. Monerie, P. Suquet, Porous materials with two populations of voids under internal pressure: I. instantaneous constitutive relations, *International Journal of Solids and Structures* 46 (3-4) (2009) 480–506.
- [18] P.-G. Vincent, P. Suquet, Y. Monerie, H. Moulinec, Effective flow surface of porous materials with two populations of voids under internal pressure: I. a gtn model, *International Journal of Plasticity* 56 (2014) 45–73.
- [19] W. Shen, D. Kondo, L. Dormieux, J. Shao, A closed-form three scale model for ductile rocks with a plastically compressible porous matrix, *Mechanics of Materials* 59 (2013) 73–86.
- [20] W. Shen, Z. He, L. Dormieux, D. Kondo, Effective strength of saturated double porous media with a drucker–prager solid phase, *International journal for numerical and analytical methods in geomechanics* 38 (3) (2014) 281–296.
- [21] A. L. Gurson, Continuum theory of ductile rupture by void nucleation and growth: Part i-yield criteria and flow rules for porous ductile media, *Journal of engineering materials and technology* 99 (1) (1977) 2–15.
- [22] S. Maghous, L. Dormieux, J. Barthélémy, Micromechanical approach to the strength properties of frictional geomaterials, *European Journal of Mechanics-A/Solids* 28 (1) (2009) 179–188.
- [23] Y.-K. Khdir, T. Kanit, F. Zaïri, M. Naït-Abdelaziz, Computational homogenization of plastic porous media with two populations of voids, *Materials Science and Engineering: A* 597 (2014) 324–330.
- [24] J. Julien, M. Gărăjeu, J.-C. Michel, A semi-analytical model for the behavior of saturated viscoplastic materials containing two populations of voids of different sizes, *International Journal of Solids and Structures* 48 (10) (2011) 1485–1498.
- [25] P.-G. Vincent, Y. Monerie, P. Suquet, Porous materials with two populations of voids under internal pressure: Ii. growth and coalescence of voids, *International Journal of Solids and Structures* 46 (3) (2009) 507 – 526.
- [26] H. Moulinec, P. Suquet, A fast numerical method for computing the linear and nonlinear mechanical properties of composites, *Comptes rendus de l’Académie des sciences. Série II, Mécanique, physique, chimie, astronomie* 318 (11) (1994) 1417–1423.
- [27] P.-G. Vincent, P. Suquet, Y. Monerie, H. Moulinec, Effective flow surface of porous materials with two populations of voids under internal pressure: Ii. full-field simulations, *International Journal of Plasticity*

56 (2014) 74 – 98.

- [28] W. Shen, J. Shao, An incremental micro-macro model for porous geomaterials with double porosity and inclusion, *International Journal of Plasticity* 83 (2016) 37–54.
- [29] C. Arson, Micro-macro mechanics of damage and healing in rocks, *Open Geomechanics* 2 (2020).
- [30] J.-F. Shao, Q.-Z. Zhu, K. Su, Modeling of creep in rock materials in terms of material degradation, *Computers and Geotechnics* 30 (7) (2003) 549–555.
- [31] J.-F. Shao, Y. Jia, D. Kondo, A.-S. Chiarelli, A coupled elastoplastic damage model for semi-brittle materials and extension to unsaturated conditions, *Mechanics of materials* 38 (3) (2006) 218–232.
- [32] M. Salari, S. Saeb, K. Willam, S. Patchet, R. Carrasco, A coupled elastoplastic damage model for geomaterials, *Computer methods in applied mechanics and engineering* 193 (27-29) (2004) 2625–2643.
- [33] H. Zhou, Y. Jia, J.-F. Shao, A unified elastic–plastic and viscoplastic damage model for quasi-brittle rocks, *International Journal of Rock Mechanics and Mining Sciences* 45 (8) (2008) 1237–1251.
- [34] F. Parisio, L. Laloui, Plastic-damage modeling of saturated quasi-brittle shales, *International Journal of Rock Mechanics and Mining Sciences* 93 (2017) 295–306.
- [35] J. Huang, M. Zhao, X. Du, F. Dai, C. Ma, J. Liu, An elasto-plastic damage model for rocks based on a new nonlinear strength criterion, *Rock Mechanics and Rock Engineering* 51 (5) (2018) 1413–1429.
- [36] Q.-Z. Zhu, D. Kondo, J.-F. Shao, Homogenization-based analysis of anisotropic damage in brittle materials with unilateral effect and interactions between microcracks, *International Journal for Numerical and Analytical Methods in Geomechanics* 33 (6) (2009) 749–772.
- [37] N. Xie, Q.-Z. Zhu, J.-F. Shao, L.-H. Xu, Micromechanical analysis of damage in saturated quasi brittle materials, *International Journal of Solids and Structures* 49 (6) (2012) 919–928.
- [38] Q. Zhu, J. Shao, A refined micromechanical damage-friction model with strength prediction for rock-like materials under compression, *International Journal of Solids and Structures* 60-61 (2015) 75 – 83.
- [39] L. Dormieux, D. Kondo, F.-J. Ulm, A micromechanical analysis of damage propagation in fluid-saturated cracked media, *Comptes Rendus Mécanique* 334 (7) (2006) 440 – 446.
- [40] M. Qi, J. Shao, A. Giraud, Q. Zhu, J. Colliat, Damage and plastic friction in initially anisotropic quasi brittle materials, *International Journal of Plasticity* 82 (2016) 260–282.
- [41] Q. Zhu, L. Zhao, J. Shao, Analytical and numerical analysis of frictional damage in quasi brittle materials, *Journal of the Mechanics and Physics of Solids* 92 (2016) 137–163.
- [42] Q. Zhu, J. Shao, Micromechanics of rock damage: Advances in the quasi-brittle field, *Journal of Rock Mechanics and Geotechnical Engineering* 9 (1) (2017) 29–40.
- [43] W. Jin, C. Arson, Micromechanics based discrete damage model with multiple non-smooth yield surfaces: Theoretical formulation, numerical implementation and engineering applications, *International Journal of Damage Mechanics* 27 (5) (2018) 611–639.
- [44] Z. P. Bazant, Nonlocal damage theory based on micromechanics of crack interactions, *Journal of Engineering Mechanics* 120 (3) (1994) 593–617.
- [45] R. H. J. Peerlings, R. De Borst, W. A. M. Brekelmans, J. H. P. DE VREE, Gradient enhanced damage for quasi-brittle materials, *International Journal for Numerical Methods in Engineering* 39 (19) (1996) 3391–3403.
- [46] N. Challamel, A variationally based nonlocal damage model to predict diffuse microcracking evolution, *International Journal of Mechanical Sciences* 52 (12) (2010) 1783 – 1800.
- [47] C. Giry, F. Dufour, J. Mazars, Stress-based nonlocal damage model, *International Journal of Solids and Structures* 48 (25-26) (2011) 3431–3443.

- [48] W. Jin, C. Arson, Nonlocal enrichment of a micromechanical damage model with tensile softening: Advantages and limitations, *Computers and Geotechnics* 94 (2018) 196 – 206.
- [49] T. Mori, K. Tanaka, Average stress in a matrix and average elastic energy of materials with misfitting inclusions, *Acta Metall.Mater* 42(7) (1973) 597–629.
- [50] J.-F. Barthélémy, L. Dormieux, A micromechanical approach to the strength criterion of drucker-prager materials reinforced by rigid inclusions, *International Journal for Numerical and Analytical Methods in Geomechanics* 28 (7-8) (2004) 565–582.
- [51] P. Baud, V. Vajdova, T.-f. Wong, Shear-enhanced compaction and strain localization: Inelastic deformation and constitutive modeling of four porous sandstones, *Journal of Geophysical Research: Solid Earth* 111 (B12) (2006).
- [52] P. Baud, S. Vinciguerra, C. David, A. Cavallo, E. Walker, T. Reuschlé, Compaction and failure in high porosity carbonates: Mechanical data and microstructural observations, in: *Rock Physics and Natural Hazards*, Springer, 2009, pp. 869–898.
- [53] W. Shen, J.-F. Shao, D. Kondo, B. Gatmiri, A micro–macro model for clayey rocks with a plastic compressible porous matrix, *International journal of plasticity* 36 (2012) 64–85.
- [54] S. Pietruszczak, D. Lydzba, J.-F. Shao, Description of creep in inherently anisotropic frictional materials, *Journal of Engineering Mechanics* 130 (6) (2004) 681–690.
- [55] N. Brantut, M. Heap, P. Meredith, P. Baud, Time-dependent cracking and brittle creep in crustal rocks: A review, *Journal of Structural Geology* 52 (2013) 17 – 43.
- [56] X. Shen, C. Arson, K. L. Ferrier, N. West, S. Dai, Mineral weathering and bedrock weakening: Modeling microscale bedrock damage under biotite weathering, *Journal of Geophysical Research: Earth Surface* 124 (11) (2019) 2623–2646.
- [57] W. Wang, T. G. Liu, J. F. Shao, Effects of acid solution on the mechanical behavior of sandstone, *Journal of Materials in Civil Engineering* 28 (1) (2016) 04015089.
- [58] W. Wang, S. Mei, Y. Cao, R. Wang, Q. Zhu, Experimental study on property modification of jointed rocks subjected to chemical corrosion, *European Journal of Environmental and Civil Engineering* 0 (0) (2020) 1–12.
- [59] L. Zhao, Q. Zhu, W. Xu, F. Dai, J.-F. Shao, A unified micromechanics-based damage model for instantaneous and time-dependent behaviors of brittle rocks, *International Journal of Rock Mechanics and Mining Sciences* 84 (2016) 187–196.
- [60] W. F. Brace, E. G. Bombolakis, A note on brittle crack growth in compression, *Journal of Geophysical Research* 68 (12) (1963) 3709–3713.
- [61] J. Shao, K. Chau, X. Feng, Modeling of anisotropic damage and creep deformation in brittle rocks, *International Journal of Rock Mechanics and Mining Sciences* 43 (4) (2006) 582 – 592.
- [62] W. Jin, C. Arson, Discrete equivalent wing crack based damage model for brittle solids, *International Journal of Solids and Structures* 110-111 (Complete) (2017) 279–293.
- [63] X. Shen, C. Arson, J. Ding, F. Chester, J. Chester, Mechanisms of anisotropy in salt rock upon microcrack propagation, *Rock Mechanics and Rock Engineering* (04 2020). doi:10.1007/s00603-020-02096-1.
- [64] H. Moulinec, P. Suquet, A fast numerical method for computing the linear and nonlinear mechanical properties of composites, *Comptes Rendus de l’Acad mie des Sciences t.318* (1994) 1417–1423.
- [65] H. Moulinec, P. Suquet, A numerical method for computing the overall response of nonlinear composites with complex microstructure, *Computer Methods in Applied Mechanics and Engineering* 157 (1998)

69–94.

- [66] G. Armand, N. Conil, J. Talandier, D. M. Seyedi, Fundamental aspects of the hydromechanical behaviour of callovo-oxfordian claystone: from experimental studies to model calibration and validation, *Computers and Geotechnics* 85 (2017) 277–286.
- [67] D. Hu, F. Zhang, J.-F. Shao, B. Gatmiri, Influences of mineralogy and water content on the mechanical properties of argillite, *Rock mechanics and rock engineering* 47 (1) (2014) 157–166.
- [68] F. Zhang, J. F. Shao, et al., Experimental study of poromechanical behavior of saturated claystone under triaxial compression, *Acta Geotechnica* 9 (2) (2014) 207–214.
- [69] Z. Liu, J. Shao, S. Xie, N. Conil, W. Zha, Effects of relative humidity and mineral compositions on creep deformation and failure of a claystone under compression, *International Journal of Rock Mechanics and Mining Sciences* 103 (2018) 68–76.
- [70] P. Leroy, A. Revil, S. Altmann, C. Tournassat, Modeling the composition of the pore water in a clay-rock geological formation (callovo-oxfordian, france), *Geochimica et Cosmochimica Acta* 71 (5) (2007) 1087 – 1097.
- [71] D. Jougnot, A. Ghorbani, A. Revil, P. Leroy, P. Cosenza, Spectral induced polarization of partially saturated clay-rocks: a mechanistic approach, *Geophysical Journal International* 180 (1) (2010) 210–224.
- [72] T. Saif, Q. Lin, A. R. Butcher, B. Bijeljic, M. J. Blunt, Multi-scale multi-dimensional microstructure imaging of oil shale pyrolysis using x-ray micro-tomography, automated ultra-high resolution sem, maps mineralogy and fib-sem, *Applied energy* 202 (2017) 628–647.
- [73] S. Monfared, F.-J. Ulm, A molecular informed poroelastic model for organic-rich, naturally occurring porous geocomposites, *Journal of the Mechanics and Physics of Solids* 88 (2016) 186–203.
- [74] L. Ma, K. G. Taylor, P. J. Dowe, L. Courtois, A. Gholinia, P. D. Lee, Multi-scale 3d characterisation of porosity and organic matter in shales with variable toc content and thermal maturity: Examples from the lublin and baltic basins, poland and lithuania, *International Journal of Coal Geology* 180 (2017) 100–112.
- [75] R. Hill, A self-consistent mechanics of composite materials, *Journal of the Mechanics and Physics of Solids* 13 (4) (1965) 213–222.